

VORTICES IN THE CO-ORBITAL REGION OF AN EMBEDDED PROTOPLANET

JOSEF KOLLER^{1,2}, HUI LI¹, AND DOUGLAS N.C. LIN³
Draft version October 29, 2018

ABSTRACT

We present global 2-D inviscid disk simulations with an embedded planet, emphasizing the non-linear dynamics in its co-orbital region. We find that the potential vorticity of the flow in this region is not conserved due to the presence of two spiral shocks produced by the planet. As the system evolves, the potential vorticity profile develops extrema (inflection points) which eventually render the flow unstable. Vortices are produced in association with the potential vorticity minima. Born in the separatrix region, these vortices experience close-encounters with the planet, consequently exerting strong torques on the planet. The existence of these vortices have important implications on understanding the migration rates of low mass planets.

Subject headings: stars: planetary systems: formation — protostellar disks — hydrodynamics

1. INTRODUCTION

The discovery of a large number of short-period extrasolar planets has generated renewed interests in the study of tidally induced migration of protoplanets in disks. The basis of migration is the gravitational interaction between a gaseous disk and an orbiting perturber, and has been analyzed well before extrasolar planets were actually discovered (Goldreich & Tremaine 1979, 1980; Lin & Papaloizou 1986a,b). It has been suggested that this tidal interaction induces the embedded protoplanet to migrate under two different circumstances. In Type I migration, the protoplanet mass is small and the disk structure is weakly perturbed. In this limit, the disk response can be analyzed with a quasi-linear approximation. Linear calculations have revealed an intrinsic imbalance of inner and outer disk torques (Ward 1997), so the planet could migrate quite quickly inward. In Type II migration, the protoplanet mass is sufficiently large for it to open up a gap in the disk (Papaloizou & Lin 1984). The protoplanet's orbital evolution is locked to the evolution of the disk, which is likely to be on the viscous timescale (Nelson et al. 2000). Both types of migration have been basically confirmed by the non-linear numerical simulations.

The high mobility of small mass protoplanets or embryo cores of giant planets from Type I migration has presented a challenge to the formation of giant planets. The absence of deep oceans is contrary to the inference that any terrestrial planet in the solar system may be formed well outside the snow-line and migrated to their present location. It is thus imperative to explore the cause which may have inhibited the Type I migration. One potential contributor to this process is the disk response to low mass planets, especially in the co-orbital region where only sketchy analytical arguments have been developed. There are, however, two notable recent exceptions. Masset (2001, 2002) has evaluated the co-orbital corotation torque and found that they can play a crucial role for the migration rate. Extensive numerical simulations of viscous disks have been performed to understand the torque dependence on the

planet mass, sound speed, disk viscosity, and the torque saturation mechanism. One generic behavior he found is that the total torque on the planet first shows an oscillation consistent with the librating fluid motion in the co-orbital region then it levels off to a constant due to the disk viscosity.

Another study is by Balmforth & Korycansky (2001), who used matched asymptotic expansions to explore the non-linear dynamics of the flows in the co-orbital region. They investigated the role of re-arranging the potential vorticity profile as a response to the planet's driving and its role in the corotation torque saturation. For inviscid flows, they also noticed the formation of vortices which they attributed to the secondary instabilities in a forced critical layer problem (the critical layer in this case is the corotation resonance).

In this *Letter*, we present results on the non-linear dynamics of the co-orbital region, based on direct, high resolution numerical simulations (§2). Our approach is quite similar to that of Masset's except that we have focused on the inviscid limit simulations. As a consequence, the total torque on the planet exhibits some interesting new behavior, instead of leveling off to a constant as in the case of viscous disks. Some of the findings are similar to what Balmforth & Korycansky have found in the excitation of vortices (§3). We provide an interpretation of why these vortices are produced in §4 and discuss the implications of our results in §5.

2. INITIAL SET-UP

We assume that the protoplanetary disk is thin and can be described by the inviscid 2-D Euler equations in a cylindrical (r, ϕ) plane with vertically integrated quantities. Two gravitating bodies, a central star and a protoplanet, are located at $r = 0$ and $r = 1$ respectively and the 2-D disk is modeled between $0.4 \leq r \leq 2$. The planet is on a fixed circular orbit at $r = 1$. The self-gravity of the disk is not included.

The mass ratio between the planet and the central star is taken to be $\mu = M_p/M_* = 10^{-4}$. Its Hill (Roche)

¹ Applied Physics Division, X-1, MS P225, Los Alamos National Laboratory, NM 87545; jkoller@lanl.gov; hli@lanl.gov² Department of Physics & Astronomy, MS-108, Rice University, Houston, TX 77005³ UCO/Lick Observatory, University of California, Santa Cruz, CA 95064; lin@ucolick.org

radius is $r_H = (\mu/3)^{1/3} = 0.032$. The disk is assumed to be isothermal with a constant temperature throughout the simulation region (i.e., it is attached to a thermal bath). The isothermal sound speed, scaled by the Keplerian rotation speed v_ϕ at $r = 1$ is $c_s/v_{\phi,r=1} = H/r$ where H is the disk scale height. We used a set of three sound speeds $c_s = 0.04, 0.05, 0.06$. In the simulations presented here, we choose an initial surface density profile with $\Sigma(r) \propto r^{-3/2}$, in order that the ratio of vorticity to surface density (potential vorticity) has a flat radial profile $\zeta = (\nabla \times \mathbf{v})_z/\Sigma \approx \text{const.}$ (Note that ζ has a small deviation from being a precise constant due to the finite pressure gradient which slightly modifies v_ϕ from its Keplerian value.) With this choice of initial condition, we avoid the generation of inflection points due to the rearrangement of ζ distribution as it is carried by the stream lines. We have also made other runs which have an initial potential vorticity gradient and we find that the results presented here also hold for them. The detailed analysis of these results will be presented elsewhere.

Since $r_H < H$ for all three different sound speeds, the planet is embedded. The planet's gravitational potential is softened by an approximate 3-D treatment. The key approach is to take the surface density at each cell spreading it out vertically based on a Gaussian density profile with a scale height determined by the local temperature. The gravitational force between the planet and the disk matter is calculated using this 3-D configuration but all the forces with the same (r, ϕ) positions are summed together. This gives a correction factor $C(r, \phi)$ to the gravitational forces, which effectively softens the gravitational potential. The torque overestimation in a 2-D geometry was studied in D'Angelo, Kley, & Henning (2003) which arises only from locations near the planet. As a test if our key finding is affected by the 3-D treatment, we excluded several Roche radii from the torque calculation and show that it is not the case.

Although there are some accumulation of gas near the planet, we do not allow any disk gas to be accreted onto it. This boundary condition is equivalent to that of sufficiently low-mass protoplanets with quasi hydrostatic envelopes (Pollack *et al.* 1996). The planet's potential is switched on over 10 orbits in order for the disk to make an adiabatic adjustment. (We have used other, longer turn-on times but the results do not depend on them.)

Simulations are carried out using a 2-D code whose basic algorithm was based on FARGO by Masset (2000) and Li *et al.* (2001). The co-rotating frame is used so that the positions of the central star and the planet are fixed at $(r, \phi) = (0, 0)$ and $(1, 0)$ (acceleration due to frame rotation is also included, see Kley (1998)). Runs are made using several radial and azimuthal grids to study the influence of resolution, and those presented here have $(n_r \times n_\phi) = 300 \times 1200$. Outflow boundary conditions are used at both the inner and outer radial boundaries. The simulations typically last several hundred orbits at $r = 1$.

One key difference between our simulations and previous studies is that our simulations are performed in the inviscid limit, i.e., we do not explicitly include a viscosity term, though numerical viscosity is inevitable and is needed to handle for example shocks. In addition, our simulations tend to be of higher resolution. With a radial

$n_r = 300$ (some runs go up to $n_r = 600, n_\phi = 2400$) and $0.4 \leq r \leq 2$, the diameter of the Hill sphere of a planet with $\mu = 10^{-4}$ is resolved by at least ~ 12 cells in each direction. Using a nested-grid technique, D'Angelo *et al.* (2002) have also made very high resolution simulations, though their simulations include an explicit viscosity.

3. TORQUE EVOLUTION

Our simulation results are generally in agreement with previous simulations for the planet on a fixed circular orbit (see Masset 2002) in terms of the generic structures produced in the disk by the tidal interactions between the planet and its surrounding flows. Since the planet mass is relatively small, only density dips are produced without gaps (at least during a few hundred orbits simulated here). We define the co-orbital region here as $|\Delta r| = |r - 1| \leq 6r_H$. The co-orbital region can be separated into several parts depending on their streamline behavior (see Masset 2002), including the horseshoe (or librating) region $|\Delta r| < r_H$, the separatrix region $r_H < |\Delta r| < \sqrt{12}r_H$, and the streaming region $|\Delta r| > \sqrt{12}r_H$. The horseshoe region can be further divided into real horseshoe streamlines enclosing all three libration points ($L_{3,4,5}$) and tadpole like streamlines enclosing either L_4 or L_5 .

Our key finding is shown in Fig. 1 which displays the total torque on the planet from the disk. It has two very distinct phases: Phase I: the total torque is negative and smooth, modulated by a period that is similar to the libration period near the L4 and L5 points ($\tau_{lib} \sim \sqrt{4/27\mu} \sim 40P$ where P is one orbit at $r = 1$). Phase II: the total torque shows very large amplitude and fast oscillations with a quasi-period of a few orbits. We see such a behavior in all the runs with three different sound speeds, though the times when the “phase” transition occurs are different. They are at $t \approx 40P, 90P$, and $210P$ for $c_s = 0.04, 0.05$ and 0.06 , respectively.

4. SHOCKS, POTENTIAL VORTICITY EVOLUTION AND INSTABILITIES

The obvious question is what causes such large amplitude and fast changes in torques. Closer inspection of the co-orbital region at times around $90P$ (using $c_s = 0.05$ as an example) reveals that vortices are generated in the separatrix region. This development is shown in Fig. 2, which depicts maps of potential vorticity ζ through the times when the system undergoes its “phase” transition. One can see that these vortices are anti-cyclones which are also blobs of higher densities (not shown here). Being in the separatrix region, they experience very close encounters with the planet repeatedly, thus exerting strong “impulses” to the planet. This results in the large amplitude and fast variations in the torque evolution.

To understand this phenomenon further, in Fig. 3, we plot the azimuthally averaged radial potential vorticity profile $\langle \zeta \rangle$ for $c_s = 0.05$ at different times $t = 0, 20P, 40P, 80P, 120P$. One sees that this profile deviates progressively away from the initially flat radial profile, developing two prominent structures at $|\Delta r| \approx 2 - 3r_H$, with a minimum at $\Delta r \approx 2.4r_H$ and a maximum at $\Delta r = 3.4r_H$. Comparing with Fig. 2, vortices apparently emerge from the minima.

The existence of the extrema (or inflection points) in the potential vorticity profile is usually regarded as a necessary condition for non-axisymmetric instabilities in rotating shear flows (Drazin & Reid 1981). The progressive steepening of this profile, say, at $\Delta r \approx 2.4r_H$ until $t < 90P$ and the subsequent flattening (see the curve at $t = 120P$) strongly suggest that there is a secondary instability which is excited around $\Delta r \approx 2.4r_H$ and vortices are the nonlinear outcome of such an instability.

How could the potential vorticity profile develop such inflection points/structures from an initially flat and stable profile? As can be seen from the evolution equation for potential vorticity

$$D(\zeta \hat{z})/Dt = (\zeta \hat{z} \cdot \nabla) \mathbf{v} = 0 \text{ in 2D,} \quad (1)$$

where D/Dt is the Lagrangian derivative, that ζ is conserved along the streamlines in 2D (Korycansky & Papaloizou 1996). Thus, the initial uniform ζ distribution should be preserved in an inviscid disk. This conclusion, however, is only true provided that streamlines can be defined everywhere in a dissipationless flow.

Disk flows in the co-orbital region around the planet, however, do not satisfy this condition (except perhaps for flows within $|\Delta r| < r_H$) because of the two sets of spiral shocks produced by the planet. These two sets of shocks emanate from close to the planet and cut through the whole disk. Flow lines which encounter these shocks are broken and the dissipation in shocks breaks the potential vorticity conservation. The consequence of the shock is equivalent to that of a strong viscous stress in the momentum equation, the curl of which, does not vanish.

To establish the role of shocks in breaking the potential vorticity conservation, we have performed three runs with different sound speeds $c_s = 0.04, 0.05, 0.06$. Even though they only span a small range, but the effects are quite clear. In Fig. 4, we plot the azimuthally averaged potential vorticity profiles for these three runs at a time just before the emergence of vortices. Vortices first appear at the minimum of the “valley” in the profiles which moves outwards as c_s increases. This growth pattern is consistent with the fact that the starting location of the shocks is also moving away from the planet when the sound speed increases.

Note that the cause for the emergence and growth of inflection points in the azimuthally averaged ζ distribution presented here is different from that due to its rearrangement along the horseshoe orbits (Balmforth and Korycansky 2001). In our calculation with a more general initial Σ (and ζ) distribution, we confirm that onset of the shearing instability occurs at an earlier epoch. The appearance of the subsequently self-excited vortices is quite similar to the development of the Kelvin-Helmholtz (KH)

instability observed at shear interfaces. A detailed study on the properties of this secondary instability, such as its threshold and growth rate, will be presented in a forthcoming paper.

5. CONCLUSIONS AND DISCUSSIONS

In this paper, we consider the tidal interaction between a protostellar disk and an embedded planet with a modest mass. Linear torque calculations suggest that such interaction leads to angular momentum transfer and inward migration of the planets. For planets with mass comparable to that of the Earth, the inferred migration time scale (Ward 1997) is much shorter than the observationally determined depletion time scale of the disk (Haisch, Lada, & Lada 2001). This analytic result raises a problem for the formation of giant planets through the core accretion process (Pollack *et al.* 1996). We reinvestigate this process in an attempt to resolve this paradox.

The embedded protoplanet induces a circulation flow pattern near its corotation region in the disk. We show here that even in disks with initially uniform potential vorticities, inflection points may emerge and grow spontaneously as potential vorticity is generated near the spiral shock in the vicinity of the protoplanet. These inflection points lead to the onset and growth of secondary instabilities.

The existence of secondary instabilities and their nonlinear outcome as vortices indicate that the flows in the co-orbital region are perhaps more complicated than linear analyses have suggested. These vortices should exert strong torques on the planet.

One limitation of our current study is that the planet is being artificially held on a fixed circular orbit. Such strong and rapidly varying torques from the vortices on the planet might cause the planet to “oscillate” and lose its phase coherence with the surrounding flow. This feedback process should have important implications for the Type I migration problem. Allowing the planet to migrate radially must be included in order to understand the planet’s response to such torques. These issues will be addressed in a forthcoming publication.

We wish to thank Neil Balmforth, Darryl Holm and Edison Liang for useful discussions. This research was performed under the auspices of the Department of Energy. It was supported by the Laboratory Directed Research and Development Program at Los Alamos and by LANL/IGPP. We are also supported in part by NASA through NAG5-11779, NAG5-9223, and NSF through AST-9987417.

REFERENCES

Balmforth, N. J. & Korycansky, D. G. 2001, MNRAS, 326, 833
 D’Angelo, G., Henning, T., & Kley, W. 2002, A&A, 385, 647
 D’Angelo, G., Kley, W., & Henning, T. 2003, ApJ, 586, 540
 Drazin, P. G. & Reid, W.H. 1981, *Hydrodynamics Stability*, Cambridge
 Goldreich, P. & Tremaine, S. 1979, ApJ, 233, 857
 — 1980, ApJ, 241, 425
 Haisch, K. E., Jr., Lada, E. A., Lada, C. J. 2001, ApJ, 553, L153
 Kley, W. 1998, A&A, 338, L37
 Korycansky, D. & Papaloizou, J.C.B. 1996, ApJS, 105, 181
 Li, H., Colgate, S. A., Wendroff, B., & Liska, R. 2001, ApJ, 551, 874
 Lin, D. N. C. & Papaloizou, J. 1986a, ApJ, 307, 395
 — 1986b, ApJ, 309, 846
 Masset, F. S. 2000, A&AS, 141, 165
 — 2001, ApJ, 558, 453
 — 2002, A&A, 387, 605
 Nelson, R. P., Papaloizou, J. C. B., Masset, F., & Kley, W. 2000, MNRAS, 318, 18
 Papaloizou, J. & Lin, D. N. C. 1984, ApJ, 285, 818
 Pollack, J. B., Hubickyj, O., Bodenheimer, P., Lissauer, J. J., Podolak, M., & Greenzweig, Y. 1996, Icarus, 124, 62
 Ward, W. R. 1997, Icarus, 126, 261

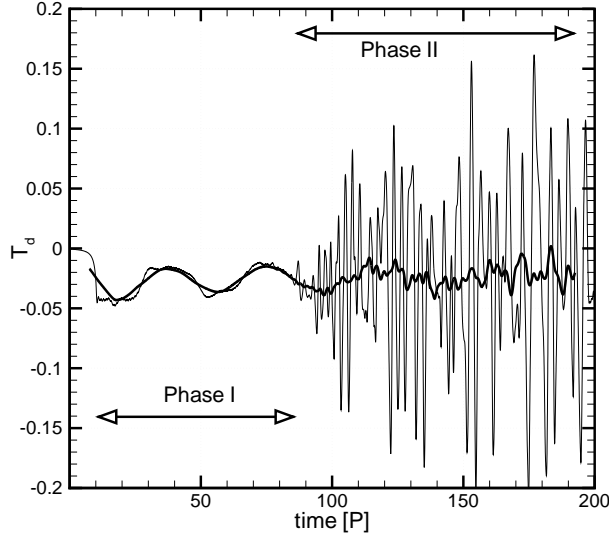


FIG. 1.— Time evolution of the total torque T_d exerted on the planet. Phase I ($t < 90P$): The total torque is negative, smooth, and shows an oscillation period of $\approx 40P$ which is consistent with the libration period. We used a turn-on time of 10 orbits for the planet mass. Phase II ($t > 90P$): The torque starts to show oscillations with increasingly high amplitudes. During the transition from Phase I to Phase II, vortices emerge around $\Delta r \approx 2.4r_H$. These vortices experience close-encounters with the planet, resulting in large amplitude variations in the torque. The bold curve depicts a moving average of T_d with a window of $t = 15P$ orbits.

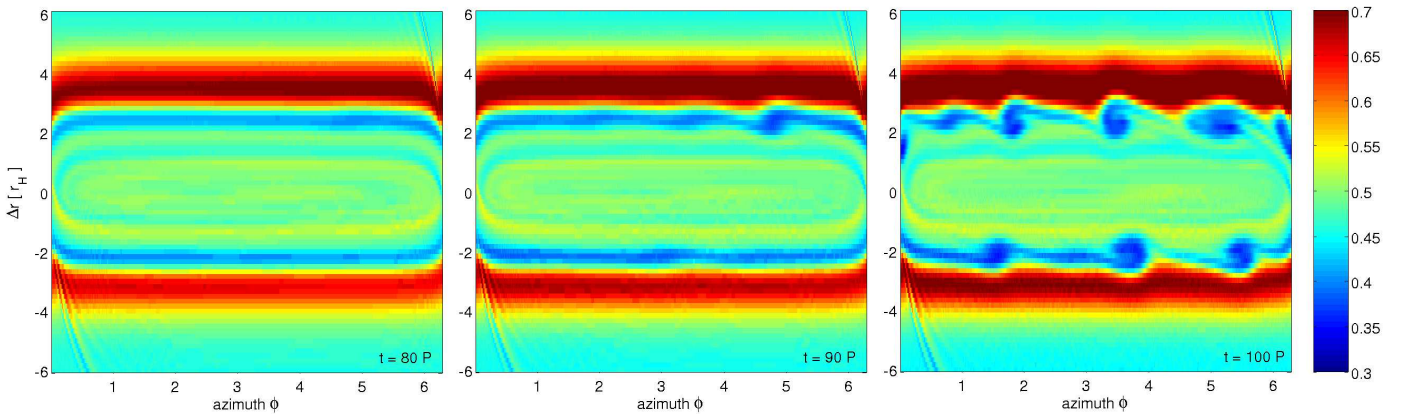


FIG. 2.— Maps of potential vorticity ζ showing the production of vortices. The planet is located at $(\Delta r, \phi) = (0, 0)$ and the radial distance to the planet is given in units of the Hill (Roche) radius r_H . Here, $c_s = 0.05$. (left) At $t = 80P$ the potential vorticity profile is relatively smooth, with two “channels” at roughly $|\Delta r| \approx 2 - 3r_H$. (middle) At $t = 90P$ the outer channel shows emerging vortices (anti-cyclones). (right) At $t = 100P$ vortices have grown to their full size in both potential vorticity channels. Note that vortices are moving in the separatrix region, so they will experience close-encounters with the planet.

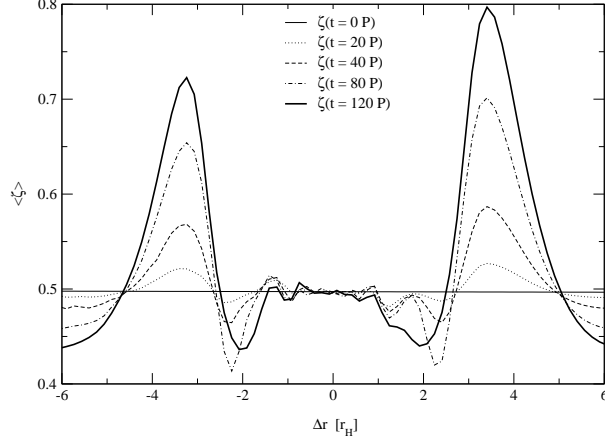


FIG. 3.— Evolution of the azimuthally averaged potential vorticity $\langle \zeta \rangle$ for $c_s = 0.05$ at different times $t = 0, 20P, 40P, 80P, 120P$. Take the structure at $\Delta r \sim 2 - 3r_H$ as an example. The profile develops dips ($\Delta r = 2.4r_H$) and peaks ($\Delta r = 3.4r_H$) progressively from $t = 0 - 80P$ until the vortices are produced at $t = 90P$, after which the minimum flattens (see the bold $t = 120P$ curve).

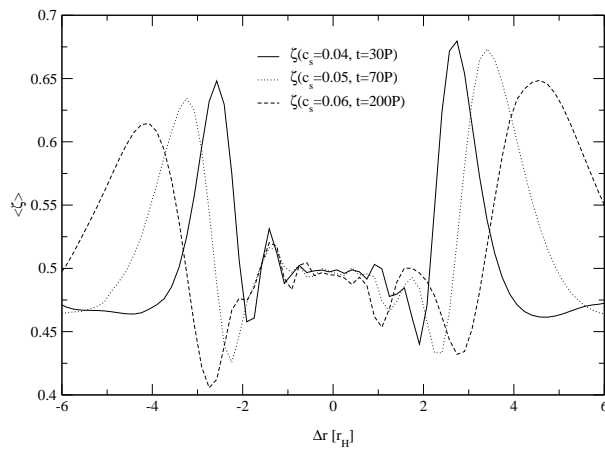


FIG. 4.— Azimuthally averaged potential vorticity $\langle \zeta \rangle$ shortly before vortices set in for different sound speeds $c_s = 0.04, 0.05, 0.06$. The evolution for lower c_s is much faster and therefore vortices develop early on. Vortices first appear at the minima of the profile. The locations of the minima move outwards proportionally as sound speeds increase, so do the starting locations of the spiral shocks.